Chapter 12
Development of Photonic Crystal Fiber-Based Gas/Chemical Sensors

Ahmmed A. Rifat, Kawsar Ahmed, Sayed Asaduzzaman, Bikash Kumar Paul and Rajib Ahmed

Abstract The development of highly sensitive and miniaturized sensors that capable of real-time analytes detection is highly desirable. Nowadays, toxic or colorless gas detection, air pollution monitoring, harmful chemical, pressure, strain, humidity, and temperature sensors based on photonic crystal fiber (PCF) are increasing rapidly due to its compact structure, fast response, and efficient light-controlling capabilities. The propagating light through the PCF can be controlled by varying the structural parameters and core–cladding materials; as a result, evanescent field can be enhanced significantly which is the main component of the PCF-based gas/chemical sensors. The aim of this chapter is to (1) describe the principle operation of PCF-based gas/chemical sensors, (2) discuss the important PCF properties for optical sensors, (3) extensively discuss the different types of microstructured optical fiber-based gas/chemical sensors, (4) study the effects of different core–cladding shapes, and fiber background materials on sensing performance, and (5) highlight the main challenges of PCF-based gas/chemical sensors and possible solutions.

Keywords Photonic crystal fiber · Optical fiber sensors · Gas sensor Chemical sensors · Optical sensing and sensors

A. A. Rifat (✉)
Nonlinear Physics Centre, Research School of Physics & Engineering, Australian National University, Acton, Act 2601, Australia
e-mail: RifatAhmmed.Aoni@anu.edu.au

K. Ahmed
Department of Information and Communication Technology, Mawlana Bhashani Science and Technology University, Santosh, Tangail 1902, Bangladesh

S. Asaduzzaman · B. K. Paul
Department of Software Engineering, Daffodil International University, Sukrabad, Dhaka 1207, Bangladesh

R. Ahmed
Nanotechnology Laboratory, School of Engineering, University of Birmingham, Birmingham B15 2TT, UK

© Springer International Publishing AG, part of Springer Nature 2019

M. F. O. Hameed and S. Obayya (eds.), *Computational Photonic Sensors*, https://doi.org/10.1007/978-3-319-76556-3_12

12.1 Introduction

Optical sensor devices have been taken as an alternative to conventional solid-state planar, brittle, less flexible, and rigid electronic devices [1]. Electronic devices have some major limitations such as high manufacturing cost, complex procedure, slower response time, and reliability as compared to the optical sensors. Electronic devices are also affected with electromagnetic (EM) and thermal noise or interference [2]. Nowadays, physical sensing based on optical platform used to sense and monitor complex environment and its surrounding such as temperature, humidity, strain, stress, pressure, and torsion having important applications in wearable sensors, robotics, health and safety monitoring [3–8]. Therefore, optical sensor devices have been found the suitable alternative for the gas, chemical, and oil-sensing applications, due to its advantages of low cost, less noise/interference, higher sensitivity, fast response, reliability, and compactness [9–11].

Since last decades, photonic crystal fiber has been shown great development in optical sensing [12–15]. Due to advance optical instrumentations, the field of fiber optics is no longer limited to telecommunication applications. PCF also known as holey fiber consists of periodically ordered microscopic cylindrical airholes running through the full length of the fiber. The standard PCF is made with fused silica (SiO_2) that has a regular pattern of voids or airholes that run parallel to its axis. Unlike traditional optical fibers, both the core and cladding are made from the same material. The structural view of PCF is shown in Fig. 12.1. Due to unique advantages of PCFs such as design freedom, light-controlling capabilities, faster detection response, and miniaturized structure, it has been received considerable attention in developing opto-devices and sensors. Moreover, modifying the structural parameters of PCFs, such as airhole diameters, pitch size, and number of rings, evanescent field can be controlled; as a result, it will find the large scale of possible applications, especially in sensing.

The first working PCF emerged from the drawing tower in late 1995. PCF was practically fabricated for the first time in 1996 by Birks et al. [16]. The first

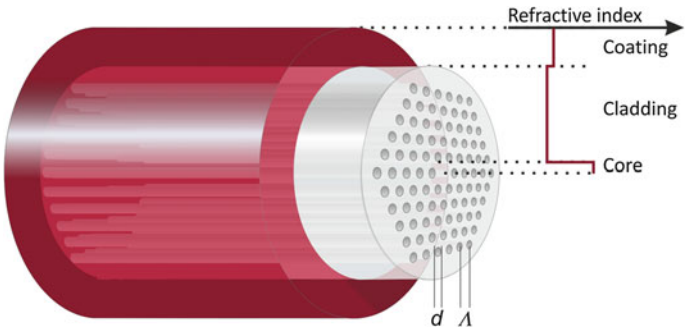

Fig. 12.1 Standard photonic crystal fiber structure

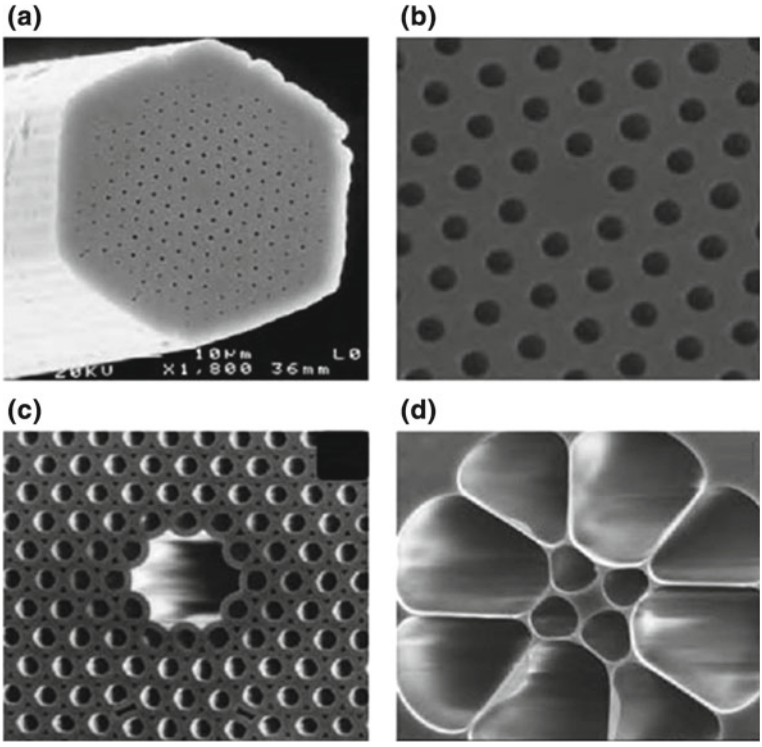

Fig. 12.2 **a** First working PCF. **b** Low loss solid core PCF. **c** The first hollow-core PCF. **d** A small core PCF extruded from Schott SF6 glass [16, 17]

fabricated PCF is shown in Fig. 12.2a. There are mainly two types of PCF, one is index-guiding PCF and another is photonic band gap (PBG) PCF. The cross-sectional diagram of index-guided photonic crystal fiber is shown in Fig. 12.2b. Photonic bandgap guiding occurs by surrounding the core of an optical fiber with the cladding region which contains airholes running along the length of the fiber. The cross-sectional diagram of photonic bandgap is shown in Fig. 12.2c. Recently, researchers are more interested in special type of PCF where both core and cladding are microstructured (see Fig. 12.2d).

Nowadays, PCF has been attracted much attention for its incredible performance and broad range of applications such as filters [18], switches [19, 20], electro-optical modulators [21, 22], polarization converters [23], and sensors [24–28]. Since last few decades, PCF has been considered and widely investigated as a suitable candidate for the optical sensing. Highly sensitive liquid and gas sensors are playing an important role in industrial processes especially for detecting toxic and flammable gases or liquids to overcome the safety issues [29]. So, it has become one of the key challenges to enhance the performance of liquid and gas sensors. Photonic crystal fiber-based liquid and gas sensors have been shown

excellent performance in terms of sensitivity response. In recent years, researchers have been shown great interest on the development of PCF-based sensors for environmental and safety monitoring [30, 31]. A wide variety of PCF-based sensing techniques have been reported by changing different geometric parameters of the PCF to get higher sensitivity, detection accuracy, and faster response time. Performance of the PCFs can be enhanced by regular or irregular geometric structure like hexagonal [32], octagonal [33], decagonal [34], square [35], honeycomb cladding [36], elliptical [37], and kagome [38]. Development of regular or irregular PCF structure leads to achieve more efficiency as well as use it in multipurpose like gas sensing, chemical sensing, bio sensing, cancer cell detection, medical science, temperature sensing, illuminations, machining, and welding applications because of its smaller size, lighter weight, chemically inertness, higher bandwidth, longer repeater span, electromagnetic immunity, and many other intriguing properties [39–41].

Researchers are trying to improve the performance of the PCF-based sensors following different geometric shape of cladding and filling different transparent material in the core and cladding. However, doping material will cause high cost and also led to the complex fabrication process. As a result, considering practical point of view, a simple PCF structure is required with high sensitivity virtues. Park et al. [42] proposed a new type of index-guided PCF to enhance sensing capability by introducing a hollow high index ring defect that consists of the central airhole surrounded by a high index GeO_2 doped SiO_2 glass ring. They showed that fraction of evanescent field was increased by increasing the diameter of central airhole; hence, the sensitivity was improved and kept the diameter smaller than cladding holes diameters for the physical realization of effective index guiding. Olyaee et al. [43] showed sensitivity 13.23% by increasing the diameter of the holes located in the inner ring and reduced confinement losses to 3.77×10^{-6} dB/m by increasing the airhole diameters located in the outer ring at the wavelength 1.33 μm. Ademgil et al. [44] proposed a microstructured core and cladding PCF for liquid sensing and found the sensitivity of 20.10% at the wavelength $\lambda = 1.33$ μm. According to the reported papers, it has been observed that both relative sensitivity and confinement loss are improved. But these are not the significant value for a gas sensor. To increase the relative sensitivity and lower the confinement loss, more research has to be done. An effective way to increase the performance of gas sensor is to design a simple PCF structure which will allow more penetration of the evanescent fields.

In this chapter, sensitivity and guiding properties of various index-guiding PCFs-based gas/chemical sensors as well as liquid sensors are extensively discussed. The finite element method (FEM) with perfectly matched boundary layer (PML) conditions is extensively used for the computational study of PCF-based gas/chemical sensors; as a result, we also described the PML effect on sensing. The important sensor parameters such as sensitivity and confinement loss effect due to change of pitch, number of rings, airhole diameters, and air filling fractions (AFF) are investigated. Recent advances of existing PCF-based gas/chemical sensors are discussed, which consist of comparisons among several PCF structures in

terms of relative sensitivity and fabrication feasibility. Finally, research gaps of this field are addressed and potential future detections to overcome them are discussed.

12.2 Fundamentals of PCF-Based Sensors

12.2.1 Sensing Mechanism of PCF-Based Sensors

The criteria's for which PCFs are used as a sensor

- **Absorbance** measured in a transparent medium.
- **Reflectance** measured in non-transparent media, usually using an immobilized indicator.
- **Luminescence** based on the measurement of the intensity of light emitted by a chemical reaction in the receptor system.
- **Fluorescence** measured as the positive emission effect caused by irradiation.
- **Refractive index** measured as the result of a change in solution composition.
- **Opto-thermal effect** based on a measurement of the thermal effect caused by light absorption.
- **Light scattering** based on effects caused by particles of definite size present in the sample.

Among these criteria's, absorbance property is widely used for sensing applications which followed by the absorption spectroscopy for practical realization. In recent years, absorption techniques are also used to detect the gas/chemicals. We have discussed the absorption spectroscopy in the following paragraph.

Fundamentals of Absorption Spectroscopy

The quality of gas assimilation lines can be utilized to perform quantitative estimation of gas. The sensitivity of the analytes is derived from the output optical power, and it is followed by the Beer–Lambert law [43, 45] as follows.

$$I(\lambda) = I_0(\lambda) \exp(-r\alpha_m lc) \tag{12.1}$$

where I_0 is the emerging optical intensity of light passing through the targeted analyte and I is the intensity of light for investigation. The relative sensitivity coefficient is r, α_m is the absorption coefficient, l is proportional to the line strength, and c is the concentration of the sample analyte.

The absorbance of the sample is defined as [25];

$$A = -\log_{10}\left(\frac{I_0}{I}\right) = r\alpha_m lc \tag{12.2}$$

Table 12.1 Absorption wavelength and line strength of some common gases [45]

Molecule	Absorption wavelength (μm)	Line strength (cm^{-2} atm^{-1})	Descriptions
Acetylene (C_2H_2)	1.533	$\sim 20 \times 10^{-2}$	Extremely flammable
Hydrogen iodide (HI)	1.541	0.775×10^{-2}	Highly toxic, colorless
Ammonia (NH_3)	1.544	0.925×10^{-2}	Toxic, irritating and destructive to tissues
Carbon monoxide (CO)	1.567	0.0575×10^{-2}	Combustion product, toxic, colorless
Carbon dioxide (CO_2)	1.573	0.048×10^{-2}	Main greenhouse gas
Hydrogen sulfide (H_2S)	1.578	0.325×10^{-2}	Toxic, colorless, flammable
Methane (CH_4)	1.667, 1.33	1.5×10^{-2}	Flammable, greenhouse gas
Hydrogen fluoride (HF)	1.330	32.5×10^{-2}	Toxic, colorless, extremely corrosive
Hydrogen bromide (HBr)	1.341	0.0525×10^{-2}	Highly toxic, colorless
Nitrogen dioxide (NO_2)	0.800	0.125×10^{-2}	Greenhouse gas
Oxygen (O_2)	0.761	0.01911×10^{-2}	Strong oxidizer, supports and vigorously accelerates combustion

The molecule shows different properties in their different states. Some gases are extremely flammable and hazardous that can be detected by PCF. The flammable gases may cause exploitation and fire in any industries as well as residential areas. Some gases are toxic that may cause different types of diseases. Few gases may cause cancer and other disorders as well. Table 12.1 shows the detailed description and absorption wavelength.

The PCF-sensing mechanism depends on the absorption lines of the corresponding gases. By the effective refractive index of the related gas which can be detected shows modal intensities at the core region. Gas species with absorption in near IR region and line strength are listed in Table 12.1. By the absorption cell, gases can be detected between any ranges of wavelength (see Fig. 12.3).

Figure 12.4 exhibits the schematic block diagram of the checked wavelength direct absorption spectroscopy system, which is used for methane ID. Light from a tenable laser source (TLS) is dispatched into a solitary mode fiber (SMF). The SMF is butt-coupled to the HC-PBF using a 3-turn positioner. An opening is left between

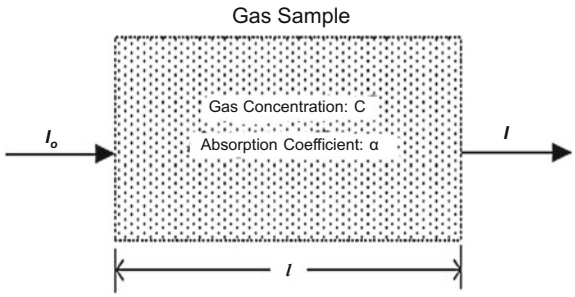

Fig. 12.3 Guided absorption cell

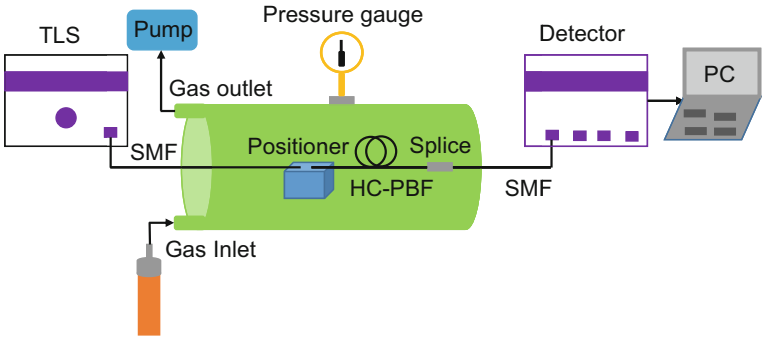

Fig. 12.4 Direct absorption spectroscopy system [46]

the terminations of the fibers to allow the gas access into the focal point of the HC-PBF. The other side of the HC-PBF is joined to a single mode fiber (SMF) using a business roundabout section splicer as described in [45]. The incapacitating of this splicer is around 1 dB. The light transmitted through the HC-PBF is measured using a Ge-identifier. A PC is used to control the tuneable laser and accumulate data from power meter which contain the locator. The open end of the HC-PBF is set in a settled vacuum chamber. Finally, a pump is used to clear the fiber before stacking with the adjusted joining of the targeted gas.

To measure the methane maintenance territory, use the two HC-PBF cells. The setup of absorption spectroscopy showed up in figure (Fig. 12.4). Consequently, the vacuum chamber is required to clear first, then it is stacked with a balanced mix of 18,750 ppmv (parts per million volumes) methane in air at a relative weight of 1 bar.

Resulting allows sufficient time for the gas to thoroughly diffuse into the fiber, and a transmission extent is recorded. The intentional territory is then established to a reach accumulated with void cells, yielding the ingestion in light of methane. From the methane maintenance band, it can be seen that the methane has generally more grounded absorption at 1331.55 nm.

12.2.2 Applications of PCF-Based Sensors

Due to unique optical properties of PCFs, it has been found large scale of potential applications. There are many applications in PCF-based sensors and some of them are listed below:

- **Gas sensor**: Gases are colorless and can be toxic. But different gas has different absorption line based on its absorption spectrum length as well as refractive index. PCF has been used to detect those colorless gases [47]. PCF-based gas sensor has the capability to detect CO that is commonly known as silent killer [43].
- **Chemical Sensor**: Chemicals are massively used in the industrial applications. In some cases, it is bounded to detect some unwanted chemical and those are poisonous for human body. Based on the internal structure of the chemical, their refractive index is also different. Each chemical has its unique refractive index like for benzene (n = 1.366), ethanol (n = 1.354), water (n = 1.33). Based on these refractive index, chemical can be detected by PCF by passing the chemical through the core region [48].
- **Biosensor**: Biosensor is a device that can sense the numerous biological molecules and/or antibodies, enzymes with the presence of associated chemical or analyte. Nowadays, PCFs are used to detect biological substances like urine glucose, pH, serum protein [49].
- **Temperature Sensor**: Temperature measurement is a key issue in industrial and environmental health monitoring purposes. The conventional temperature measurement mechanism is not suitable. PCF-based temperature sensors are most popular for temperature sensing because of its simple and cost-effective detection capabilities. To date, several number of PCF-based temperature sensors have been reported [50, 51].
- **Refractive Index Sensor**: Refractive index-based sensors are vastly using in optical sensing area. Based on the refractive index of different specimen, different applications are already employed among them surface plasmon resonance (SPR) is notable [52, 53].
- **Corrosion Sensor**: The deterioration and loss of a material are commonly known as corrosion. With the development of PCF-based corrosion sensors, it can be easily monitored the present structural condition of aircraft [54], steel [55], and other materials.
- **Pressure Sensor**: Pressure is a common behavior in case of gaseous and liquid chemicals. Moreover the revolutionary changes in the optical field, PCF-based pressure sensor played the significant role by measuring the pressure inside the patient body especially for urodynamic and cardiovascular assessment [56].
- **Humidity and Moister Sensor**: To predict the present state of the atmospheric condition some weather forecasting parameters are needed to be calculated. Among them, humidity is exceedingly crucial. Nowadays, PCF-based humidity and pressure sensors are using widely [57, 58].

- **Flying Particle Sensor**: Different particles are generally present in the environment (like in open air). But the particles are too tiny that it cannot be easily detected. Some radioactive substance may be present in the different areas air, and those are flying randomly. This type of sensor can be used in radioactive areas to monitor the environment [59].
- **Transverse Load Sensing**: Utilizing the mechanism of light propagation property load can be sensed. Optical fiber can directly use to sense load in the transverse direction [60].

12.2.3 Advantages of PCF-Based Sensors

By varying PCF structure (like hexagonal, octagonal, decagonal) and also varying the structural core–cladding size with different arrangement, propagating light can be tailored significantly. For the PCF-based sensors, evanescent field is the key element. Due to PCFs light-controlling capability, evanescent field can be tailored intensely; as a result, sensor performance can be improved significantly.

12.2.4 Optical/Guiding Properties of PCF Sensors

The better optical guiding properties ensure the application of PCFs as gas/chemical sensors. Optical properties are the core area of research on PCF. The sensor guiding properties of the PCFs are discussed below stepwise in details [12, 61].

Relative Sensitivity

First and foremost nature of a PCF used as sensor is needed to compute the relative sensitivity response. Relative sensitivity response of a PCF denoted the sensing capacity of the proposed PCF. Relative sensitivity is symbolized by r, and it can be calculated through the following equation [47];

$$r = \frac{n_s}{\mathrm{Re}[n_{eff}]} f \tag{12.3}$$

where n_s is the refractive index of target gas species, typically consider as 1 and Re [n_{eff}] is the real part of the effective mode index. Here, f is the fraction of holes power by total optical power which can be defined as [62]:

$$f = \frac{\int_{holes} \mathrm{Re}(E_x H_y - E_y H_x) dxdy}{\int_{total} \mathrm{Re}(E_x H_y - E_y H_x) dxdy} \tag{12.4}$$

Here, E_x, E_y, H_x, and H_y are the transverse electric and magnetic field of the guided mode, respectively.

Confinement loss

Confinement loss or leakage loss occurs due to leaky nature of the mode and irregular arrangement of airholes. Those airholes are playing the role of dielectric medium. Confinement loss also depends on transmitted wavelength, parameter shape and size, number of holes, and rings. A circular-shaped anisotropic perfectly matched layer (C-APML) is used to satisfy the boundary condition which avoids unwanted electromagnetic reflection at the boundary of PCF. By this term, confinement loss or leakage loss can be calculated by the imaginary part of the effective refractive index. The confinement loss or leakage loss can be calculated by the following equation [63]:

$$L_c(\mathrm{dB/m}) = 8.686\, K_0 Im\left(n_{eff}\right) \times 10^6 \tag{12.5}$$

where $K_0 = 2\pi/\lambda$, is the wave number and $Im[n_{eff}]$ is the imaginary part of the effective refractive index.

Birefringence

Birefringence is one of the crucial properties of PCFs. It is highly influential for polarization maintaining fiber (PMF). Birefringence is a property of a PCF which comes from some geometric asymmetry based on airholes position. Highly structural asymmetry of PCF, especially first ring of the PCF, produces higher order of birefringence, and structural symmetry of PCF has no influence to produce birefringence. The mathematical formulation of birefringence can be expressed as [64],

$$B(\lambda) = \left| n_{eff}^{x} - n_{eff}^{y} \right| \tag{12.6}$$

Beat length

Another wavelength-dependent parameter is beat length. Beat length is a significant argument to discover the birefringent optical fibers. It defines the optical signal transmission length along the fiber when the phase difference of two orthogonal polarization states varies 360° or 2π radians. This property leads to periodic power exchange between two orthogonal components. This period is called beat length which can be evaluated by the following expression [65]:

$$L_B(\lambda) = \frac{\lambda}{B(\lambda)} \tag{12.7}$$

V-Parameter

A PCF can be single mode or multimode. A cutoff value always present there for determining the fiber for modal analysis. If the value of V is less than or equal to 2.405, then it indicates the single mode operations; otherwise, it permits multimode

operations. The single mode response for step index fiber can be determined by the V-parameter which is defined by [66]:

$$V_{eff} = \frac{2\pi}{\lambda} a \sqrt{n_{co}^2 - n_{cl}^2} \tag{12.8}$$

Here, n_{co} and n_{cl} are the refractive index of core and cladding; a is the radius of the fiber core. The fraction of optical power in a certain mode is bounded inside a fiber core determined by V number. The lower V-value indicates the optical power fraction is low and vice versa.

Effective Area

Effective mode area is generally considered as the light carrying region. For fundamental propagating mode, electric field (E) distribution occurs inside the core; as a result, effective mode area (EMA) of a PCF can be determined by the following equation [32]:

$$A_{eff} = \frac{\left(\iint |E(x,y)|^2 dxdy\right)^2}{\iint |E(x,y)|^4 dxdy} \tag{12.9}$$

For high bit rate data transmission system (especially for telecommunication), large effective mode area is required. On the contrary, lower EMA is preferable for nonlinear applications.

Nonlinearity

High-optical power density is provided by a small effective area for which the nonlinear effects would be significant. The nonlinear effective or nonlinearity is closely related with the effective area and also nonlinear coefficient of the PCF background material in associated with the operating wavelength λ. The nonlinear coefficient can be examined by the following equation [32]:

$$\gamma = \left(\frac{2\pi}{\lambda}\right)\left(\frac{n_2}{A_{eff}}\right) \tag{12.10}$$

where n_2 is the nonlinear refractive index. Nonlinear effects are very advantageous in different optical devices and optical applications such as broadband amplification, channel demultiplexing, wavelength conversion, soliton formation, optical switching and many more applications. Nevertheless, higher orders of nonlinearity are responsible for supercontinuum generation (SCG).

Splice Loss

Splice loss is another important parameter for fiber design consideration. Generally, for longer distance signal carrying or longer distance optical communication aspect

two fibers are experienced by joining or splicing. It is very sensitive issue because due to small mismatch of the fibers during the splicing will led to the large signal attenuation. Splice loss occurs during the splicing between PCF and the single mode fiber. Splice loss can be calculated by the following equation [32]:

$$L_S = -20\log_{10}\frac{2W_{SMF}W_{PCF}}{W_{SMF}^2 + W_{PCF}^2} \tag{12.11}$$

where W_{SMF} and W_{PCF} are the mode field diameters of the single mode fiber and PCF, respectively.

Refractive Index

Transparent materials are highly used for PCF fabrication. The common transparent material silica has been used extensively for the PCF fabrication. Even as a standard PCF, silica fiber has been considered till now. Due to the technological advancement, different types of transparent materials such as tellurite, graphene, ZBLAN, and TOPAS have also been shown great interest. These are all the basic material characteristics which completely depend on refractive index. Refractive index is a material itself property which can be increased or decreased by doping other materials based on the different applications.

12.3 Overview of PCF-Based Gas/Chemical Sensors

12.3.1 Conventional Optical Fiber Sensors

Optical fiber-based surface plasmon resonance (SPR) sensor has been reported by Mishra et al. [67], for the detection of hydrogen sulfide gas. The schematic diagram of the experimental setup is shown in Fig. 12.5. To utilize the SPR-based gas sensor, nickel oxide doped ITO thin film has been used. Gas chamber having the facility with inlet and outlet was used, and the fiber probe was inserted into the gas chamber. The unpolarized light lunched at one end of the fiber and at the other end of the fiber is connected to the spectrometer. To study the SPR response of the hydrogen sulfide gas, the gas chamber was evacuated with the help of a rotary pump and the reference signal was recorded.

Recently, optical fiber-based SPR sensor for the detection of ammonia gas has also been reported [68]. The sensitivity of the sensor with optimized thickness of BCP layer is 1.891 nm/ppm and is larger than the sensitivity values obtained in the cases of Ag/BCP and Cu/BCP-coated probes for the concentration range 1–10 ppm of the ammonia gas.

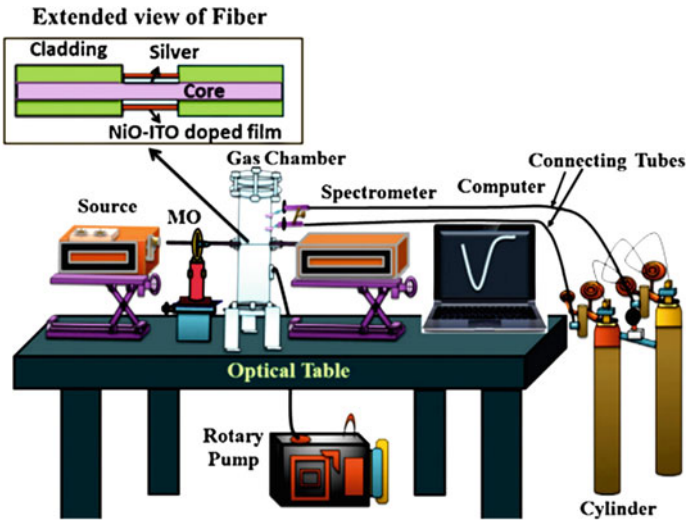

Fig. 12.5 Conventional optical fiber sensor [67]

12.3.2 PCF-Based Sensors

Based on geometrical structure, different types of PCFs have been reported for the gas/chemical sensing. The most common and modest PCF-based sensor structure is hexagonal structure. Moreover, circular, square, octagonal structures have also been reported. These types of shapes are constructed based on the orientation of airholes

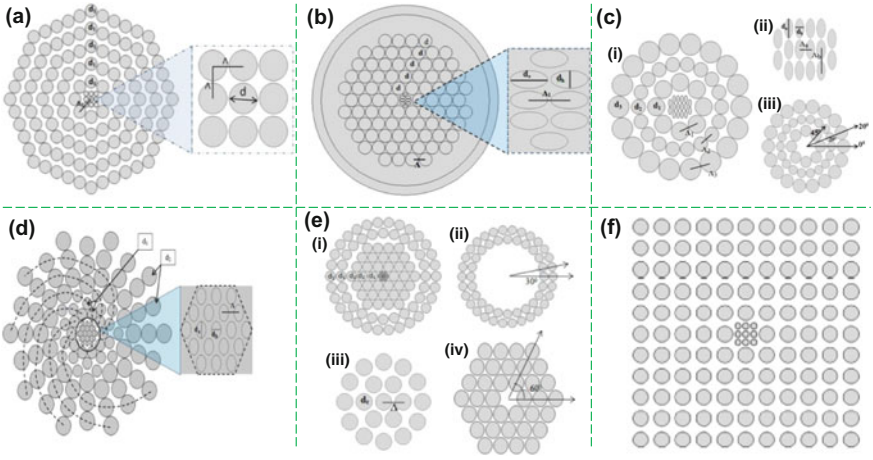

Fig. 12.6 Different types of PCF-based sensors. **a** Octagonal, **b** hexagonal, **c** hybrid, **d** spiral, **e** hybrid combined, and **f** Square

in the cladding region. For the various architectural shapes, light guiding mechanism through the fiber may have different manner. Here, from the design prospective, different types of PCF-based sensor are shown in Fig. 12.6. Figure 12.6 shows the different types of PCF such as octagonal (Fig. 12.6a), hexagonal (Fig. 12.6b), hybrid (Fig. 12.6c), spiral (Fig. 12.6d), hybrid combined (Fig. 12.6e), and square (Fig. 12.6f)-based chemical/gas sensors.

12.4 Guiding Properties Controlling Parameters of PCFs

Guiding properties or so-called optical properties can be controlled by some fundamental parameters of PCF. By recent vibrating research, it has been concluded that pitch, air filling ratio, diameters of airholes of both core and cladding significantly affect the result of wave guiding properties. In this section, a brief discussion on the sensor performance controlling parameters and their effects have been outlined.

12.4.1 Pitch Effects on Sensing

In PCF, airholes exists through the entire fiber; those are forming on silica background. These airholes are organized in a well-defined geometrical pattern. The hole-to-hole distance more specifically center-to-center distance of two adjacent airholes is called pitch (see Fig. 12.7). By altering, pitch sensitivity of PCFs can improve.

Figure 12.8 shows the pitch effect on relative sensitivity of PCF. The figures (see Fig. 12.8a–c) illustrates that smaller the pitch led to the higher relative sensitivity because the lower pitch value induces the lower space between airholes which result congested airholes. These airholes direct the evanescent field through the core region.

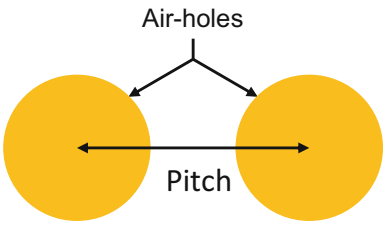

Fig. 12.7 Pitch of PCF

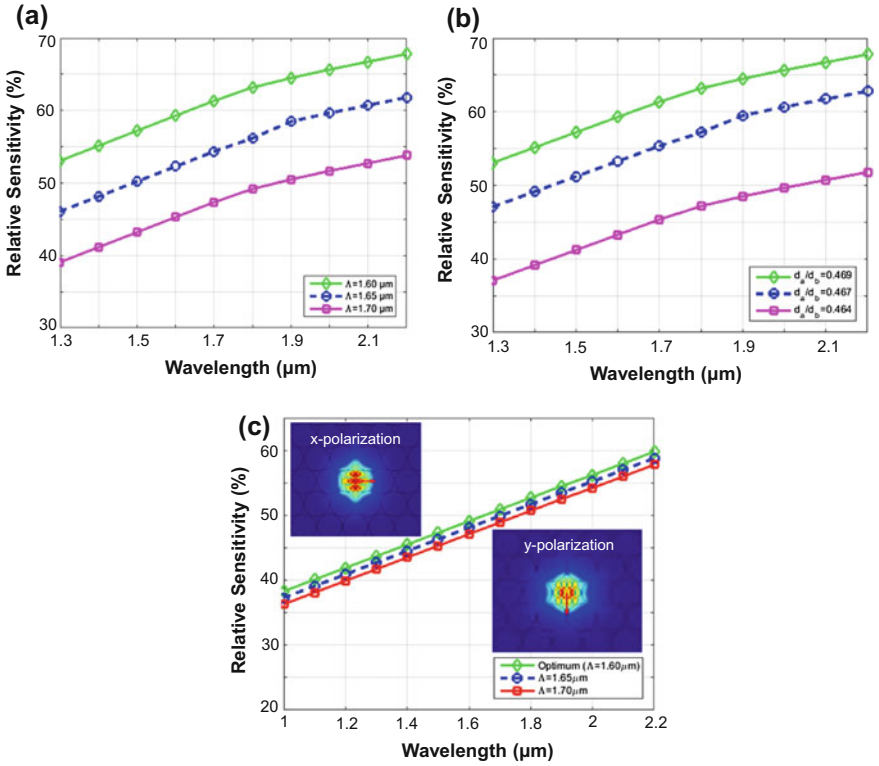

Fig. 12.8 Analysis the pitch effect on relative sensitivity of PCF [12]

12.4.2 Diameter Effects on Sensing

Diameter has significant effects on relative sensitivity. These diameters mean air-holes diameter of core region as well as cladding region. By changing the diameters, relative sensitivity can be tailored. In Fig. 12.9a, b, it is observed that the larger diameters show higher relative sensitivity.

12.4.3 Air Filling Ratio Effects on Sensing

Air filling ratio is the ratio between diameters of airhole and pitch. The air filling ratio is another controlling parameter of relative sensitivity of PCF sensors. By changing both diameter and pitch at a certain ratio together air filling ratio changes, there exists a cutoff air filling ratio which is require to maintain. The cutoff value of the air filling ratio is set as level of 0.95. Figure 12.10 illustrates that relative

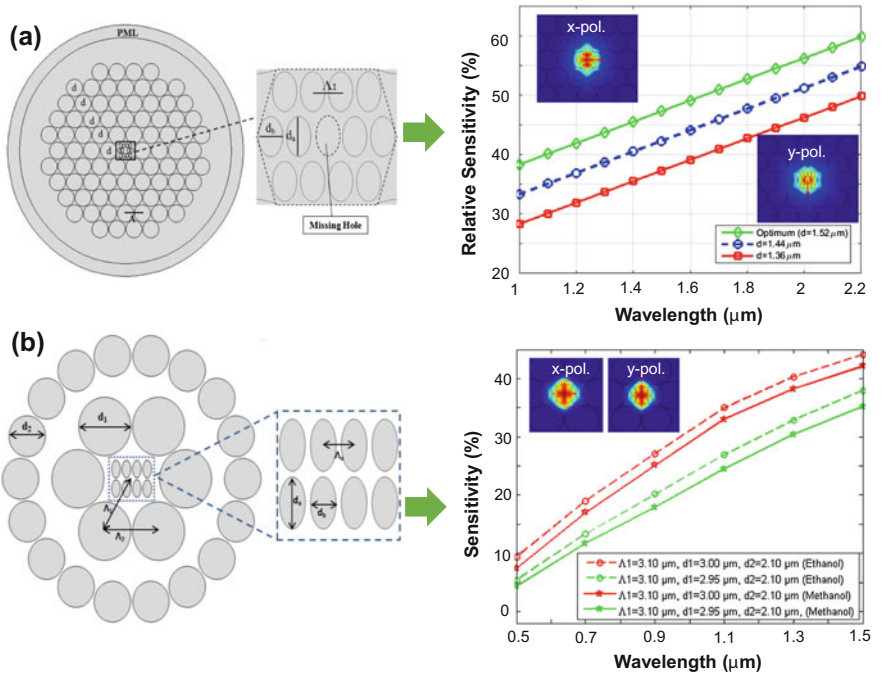

Fig. 12.9 Analysis the diameter effect on relative sensitivity with **a** hexagonal PCF, **b** hybrid PCF [12, 69]

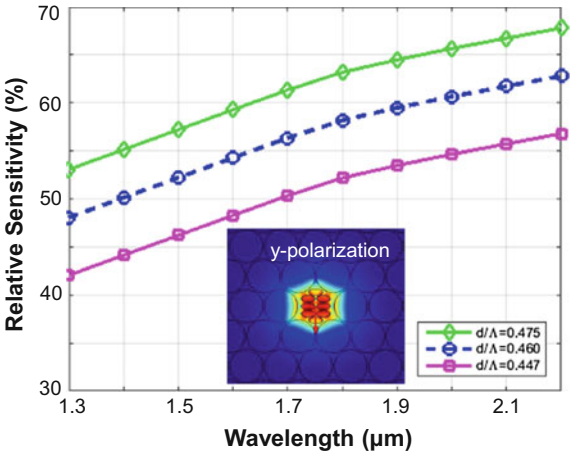

Fig. 12.10 Analysis the effect of air filling ratio on relative sensitivity of PCF [47]

sensitivity changes a lot due to small change of air filling ratio. The air filling ratio can define by the following equation

$$\text{Air filling ratio} = \frac{d(Diameter)}{\Lambda(pitch)} \tag{12.12}$$

12.5 Core-Shaped Effects on Sensing

In PCF-based gas/chemical sensors, core is a key parameter in terms of sensor performance. Generally, gases and chemicals are filled through the core; as a result, core shape has effects on sensing. According to Fig. 12.11, it is visible that an elliptical hole in a rhombic orientation shows the higher sensitivity responses than the other orientation of airholes at the innermost core region.

12.5.1 Hollow-Core PCF-Based Sensors

Recently, a simple hollow-core PCF (HC-PCF) where core is doped with different material which has been reported for gas sensing [70] (see Fig. 12.12a). The operating wavelength varied from 0.8 to 1.60 μm to investigate the different guiding properties. At wavelength λ = 1.60 μm, it shows the maximum sensitivity response of 19.94% (Fig. 12.12b) and at the same time, it also reduces the confinement loss to 2.74×10^{-4} dB/m.

A hybrid structure photonic crystal fiber-based gas sensor is presented in Fig. 12.13a to detect toxic and colorless gases. Numerical study showed that

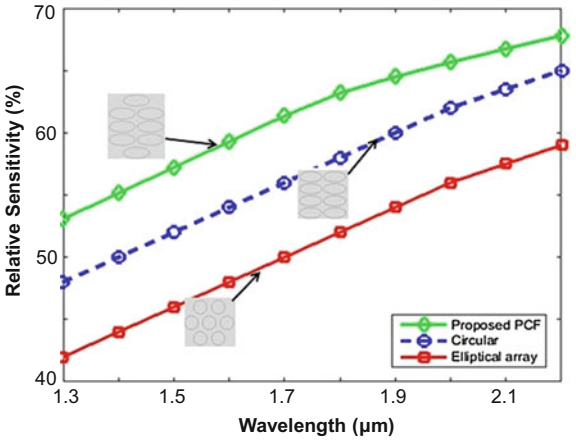

Fig. 12.11 Core shape effect on relative sensitivity [47]

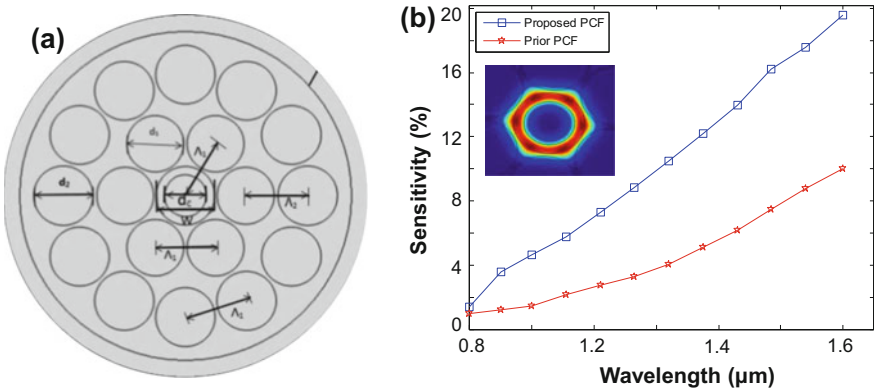

Fig. 12.12 **a** Cross-sectional view of doped material-based hollow-core PCF. **b** Sensitivity as a function of wavelength [70]

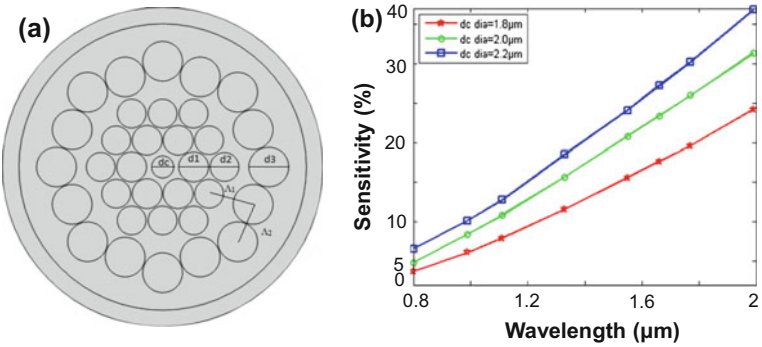

Fig. 12.13 **a** Cross-sectional view of hollow-core-based hybrid PCF. **b** Sensitivity as a function of wavelength

sensitivity response of this hybrid PCF sensor enhanced to 15.67% (Fig. 12.13b). The confinement loss or leakage loss decreased to 1.12×10^{-7} dB/m by acquainting an octagonal ring of airholes in the outer cladding. This sensor works in wider range of wavelength from 0.8 to 2 μm.

Two different structures of HC-PCF have been presented in Fig. 12.14a, b [71]. The numerical result shows that hexagonal PCF (consist with six airholes in the first ring) shows 2.22 times higher sensitivity responses compared to the octagonal PCF (consist with eight airholes in the first ring) (Fig. 12.14c). Octagonal PCF also exhibits low confinement loss. These PCFs have been reported to sense the lower refractive index-based gases (toxic/flammable) at a wide range of wavelength from 0.8 to 2 μm [71].

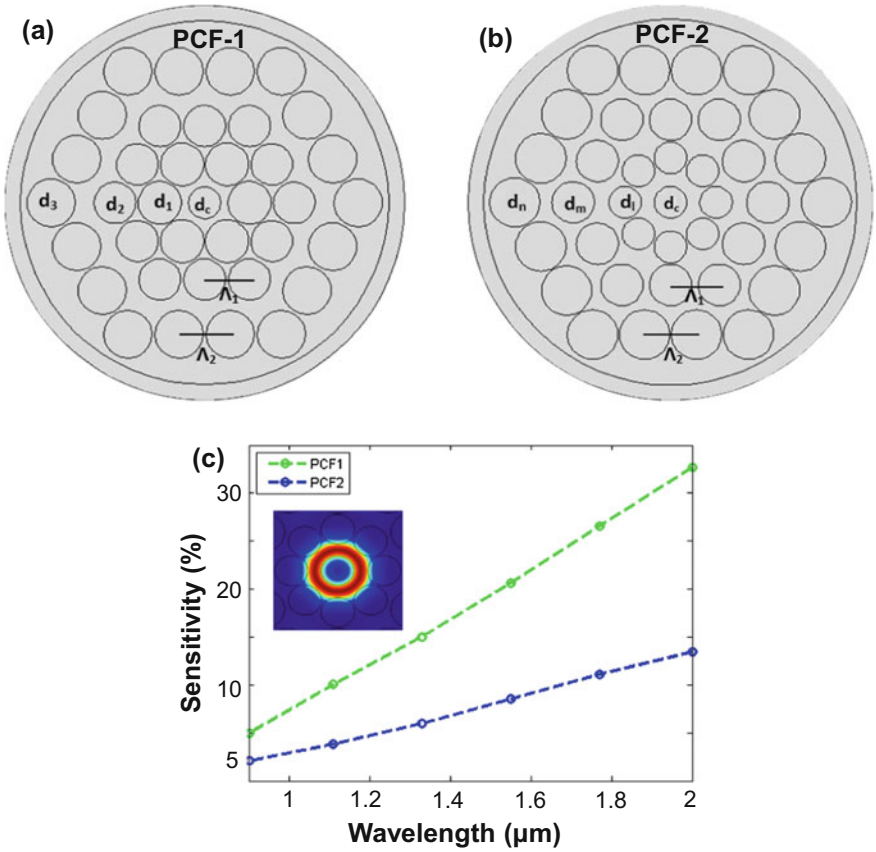

Fig. 12.14 Cross-sectional view of **a** hexagonal, **b** octagonal PCF, and **c** comparison of two HC-PCFs based on sensitivity [71]

12.5.2 Slotted-Core PCF-Based Sensors

Slotted-core PCF is widely used in terahertz communication applications. However, recently it shows great interest in sensing applications as well. Recently, Asaduzzaman et al. reported a slotted-core PCF for gas sensing (Fig. 12.15a) [72]. Numerical result reveals that slotted-core PCF is more suitable for the sensing application, and it shows the maximum relative sensitivity of 48.26%. By using slotted-shaped airholes, relative sensitivity response increased a lot than the prior PCFs which is presented in Fig. 12.15b.

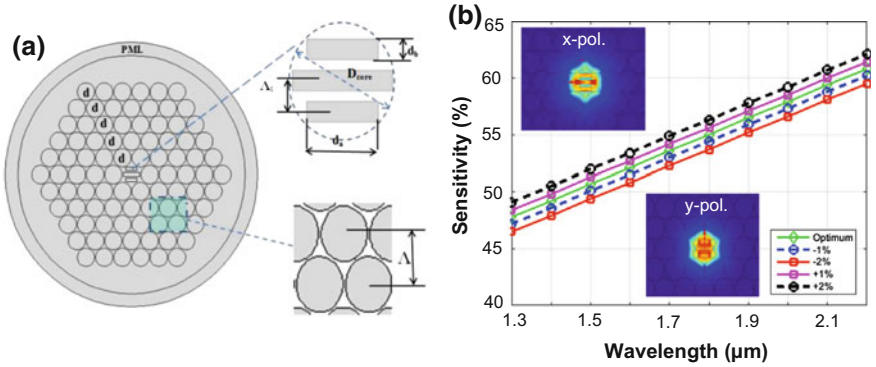

Fig. 12.15 **a** Cross-sectional view of slotted-core PCF. **b** Sensitivity as a function of wavelength (inset shows the x- and y-polarized modes) [72]

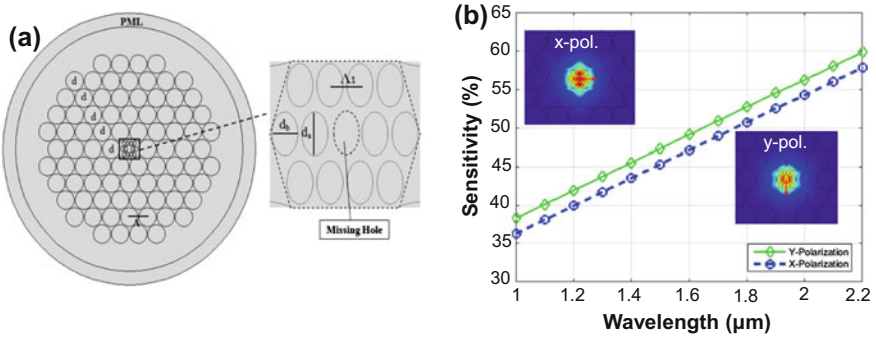

Fig. 12.16 **a** Cross-sectional view of microarray core-based PCF and **b** sensitivity as a function of wavelength [29]

12.5.3 Microstructured Core PCF-Based Sensors

Recently, PCF with microarray pattern core has been reported by Asaduzzaman et al. [12] (Fig. 12.16a). The core region contains vertically arranged elliptical holes which enhanced the relative sensitivity responses. The elliptical holes are arranged in hexagonal shape with missing holes at center. It shows the maximum sensitivity response of 43.7% (Fig. 12.16b). The structural geometric parameters also tuned to optimize the sensor performance.

Asaduzzaman et al. [47] reported a microcore PCF-based gas sensor for detecting colorless or toxic gases and monitoring air pollution by measuring gas condensate components in production facilities (Fig. 12.17a). According to the computational results, the high relative sensitivity response of 53.07% is obtained at 1.33-μm wavelength for optimum parameters which is shown in Fig. 12.17b. Here,

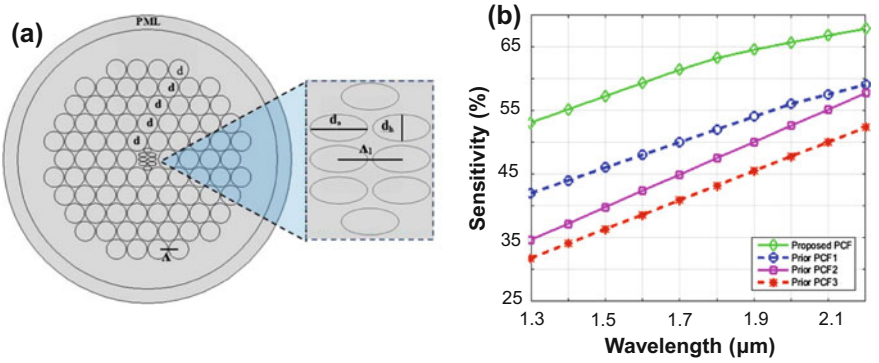

Fig. 12.17 **a** Elliptical holes array core-based PCF and **b** sensitivity as a function of wavelength [47]

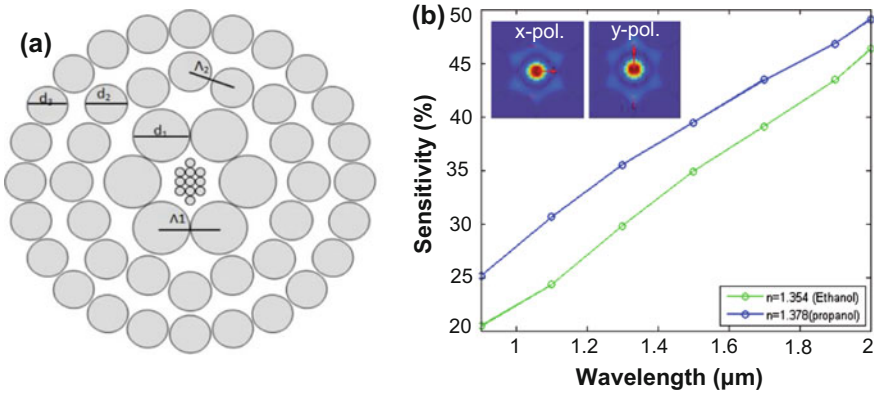

Fig. 12.18 **a** Cross-sectional view of PCF with microarray-circular hole-based core and **b** sensitivity as a function of wavelength [73]

elliptical-shaped holes are arranged in an elliptical manner which led to the higher sensitivity response than the previous reported sensor [47].

A circular photonic crystal fiber (C-PCF)-based chemical sensor presented in Fig. 12.18a [73]. It investigated the detection of ethanol and propanol chemical compound. For both chemicals (n = 1.354, n = 1.378), proposed C-PCF sensor shows higher relative sensitivity response compared to reported results in Fig. 12.12b and Fig. 12.14b (Fig. 12.18b).

12.6 Cladding Effects on Sensing

Cladding is the outer layer of photonic crystal fibers which helps to concentrate light through the core region. Cladding has significant influence in reducing confinement loss and guiding light to pass through the center core which may result more power at core region. Shape of cladding means the different geometrical organization of airholes surrounding the core region. Different cladding shape has very small impact on PCF-based gas sensing. Different cladding structure-based PCF gas sensors are shown in Fig. 12.19. It is visible that hybrid shape PCF shows better relative sensitivity compared to the circular PCF [74]. Hybrid means asymmetric arrangement of airholes at cladding region such as hexagonal, octagonal, or in circular manner.

Cladding air filling ratio also affects the relative sensitivity. Figure 12.20 reveals that higher air filling ratio introduces the higher relative sensitivity which increases with respect to wavelength.

Cladding airhole diameters are also responsible for changing in relative sensitivity. The larger airhole at outer layer of cladding reduces the confinement loss but has very less effects on relative sensitivity. On the other hand, larger airhole at inner most layer of cladding increases the sensitivity but no significant effects on confinement loss. Besides, the increment of airhole diameters in cladding increases the relative sensitivity which shows in Fig. 12.21.

Figure 12.22 exhibits the effects of inner layer and outer layer airholes effects on the relative sensitivity. According to Fig. 12.22b, it is clearly visible that first-cladding layer airhole diameters have significant effects on sensing. With the increase of first airhole diameters, sensitivity increases significantly. On the contrary, third-layer/ring diameter variation has no significant effects on sensing (Fig. 12.22c).

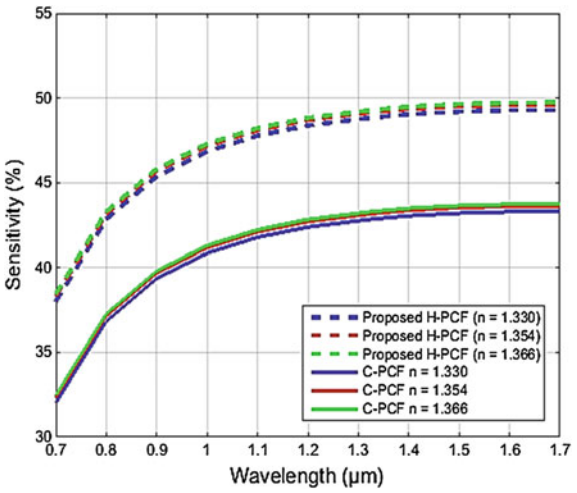

Fig. 12.19 Cladding shape effects on relative sensitivity [74]

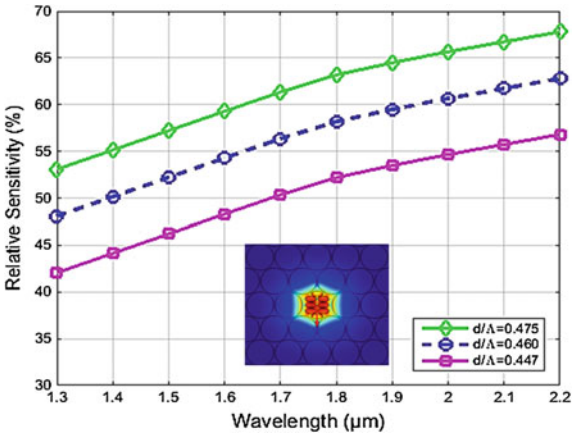

Fig. 12.20 Cladding air filling ratio effect on relative sensitivity [47]

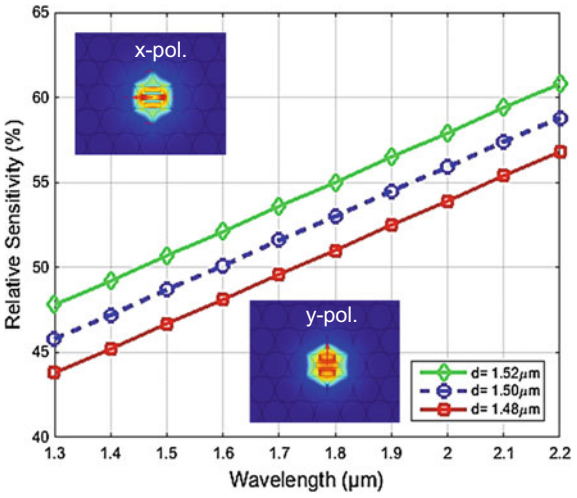

Fig. 12.21 Analysis the cladding diameter effect on relative sensitivity [72]

According to Fig. 12.23, it is also agree with the previous argument that first cladding layer is the important layer which has substantial effects on sensing performance. Figure 12.23a shows a two-ring-based hybrid PCF. Figure 12.23b shows the two different cases, one is for ethanol and another one is methanol gas. Both cases show the same result that due to increase in first layer airhole diameters, sensitivity increases significantly.

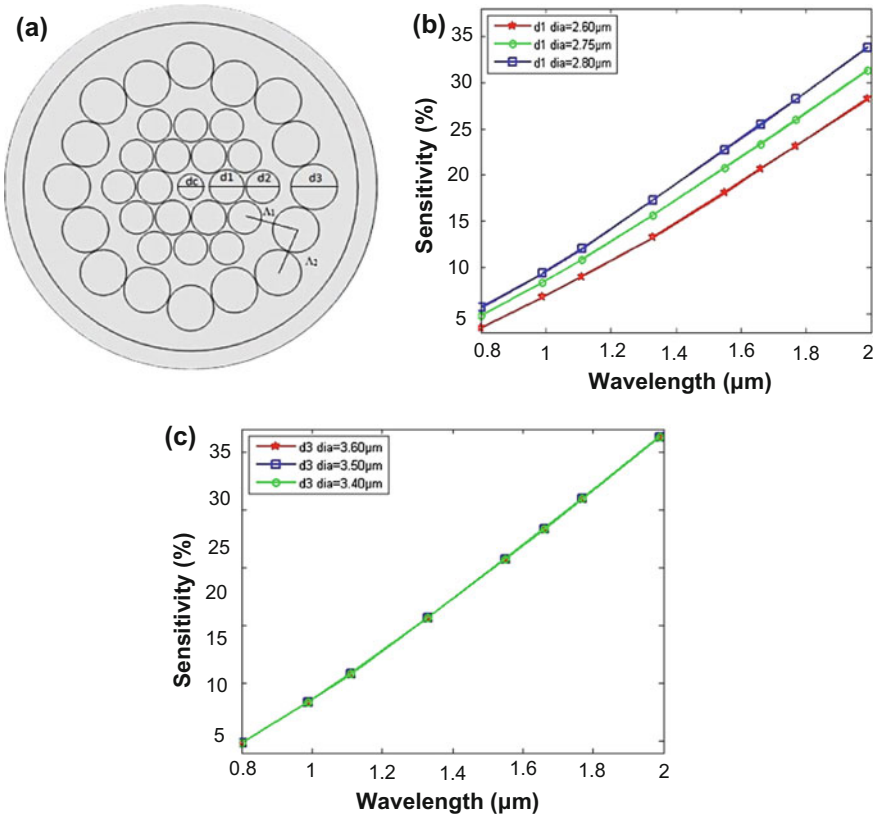

Fig. 12.22 **a** Cross-sectional view of hybrid PCF, **b**, and **c** cladding diameter (layer-based) effects on relative sensitivity

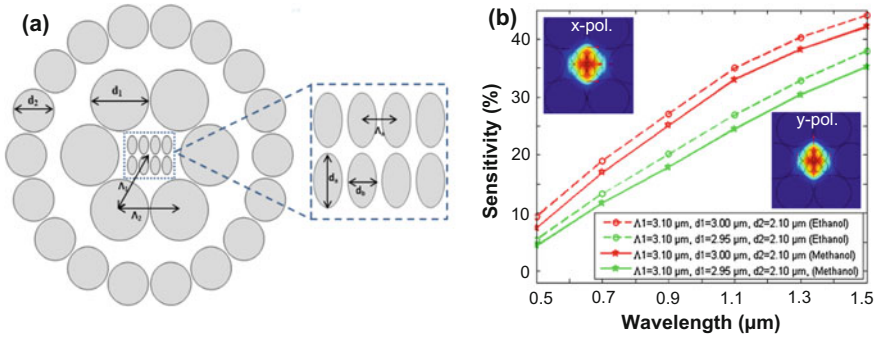

Fig. 12.23 **a** Cross-sectional view of two-ring hybrid PCF and **b** sensitivity effects due to change of first layer cladding diameters [69]

12.7 Perfectly Matched Layer (PML) Effects on Sensing

Perfectly matched layer is an artificial layer that was primarily developed by the researcher Berenger [75]. It is the outermost layer of the PCF that enclosed the cladding region. Absorption boundary layer is needed to diminish the incident unwanted electromagnetic radiation which employs the role of absorption boundary condition (ABC) [76]. Generally, PCF-based gas/chemical sensors depth is set as 10% of the cladding region. The width of the PML does not have much effects on sensitivity response. However, it has effects on confinement loss measurement [77].

12.8 Fiber Background Material Effects on Sensing

Recently, Kawsar et al. [78] investigated the effect of background materials on sensing performance (Fig. 12.24). Figure 12.24a shows the cross-sectional view of the reported sensor structure. It focuses the effect of background material on relative sensitivity at the operating wavelength 1.2–2 μm wavelength. The relative sensitivity rapidly increases with respect to wavelength. Normally, silica is used as a background material. However, they explored three different materials such as crown glass, silica, and ZBLAN as background materials with tiny airholes in core regions. From Fig. 12.24b, it can be illustrated that although, initially, silica shows the highest sensing performance, after crossing the operating wavelength 1.6 μm, ZBLAN shows the maximum sensitivity. The core-guided fundamental mode with x- and y-polarization for background material crown glass (i and ii), silica (iii and iv), and ZBLAN (v and vi) is shown in Fig. 12.24c. Finally, it can be said that background materials also have strong influence on sensor performance.

12.9 Future Directions and Conclusions

In this chapter, we discuss the optical properties of PCF and working principle of PCF-based gas/chemical sensors. We also extensively discuss the different types of PCF-based gas/chemical sensors and also the effects of core–cladding and background materials on the sensing performance. The conventional PCF can be fabricated by following the standard stack-and-draw fiber fabrication method [79]. However, irregular PCF such as octagonal, decagonal, circular, kagome, and hybrid structures fabrication is still challenging. Although the fabrication of irregular PCFs is complex, nowadays it can be done by different fiber fabrication techniques. Sol–gel technique [80] is a modern innovation for PCF fabrication which enables to contrast diameter and pitch of any size of airholes. Besides, sol–gel casting [81], extrusion [82], drilling [83] methods are suitable alternative to fabricate such irregular PCF structure. The use of chemical and gas sensors in industries is

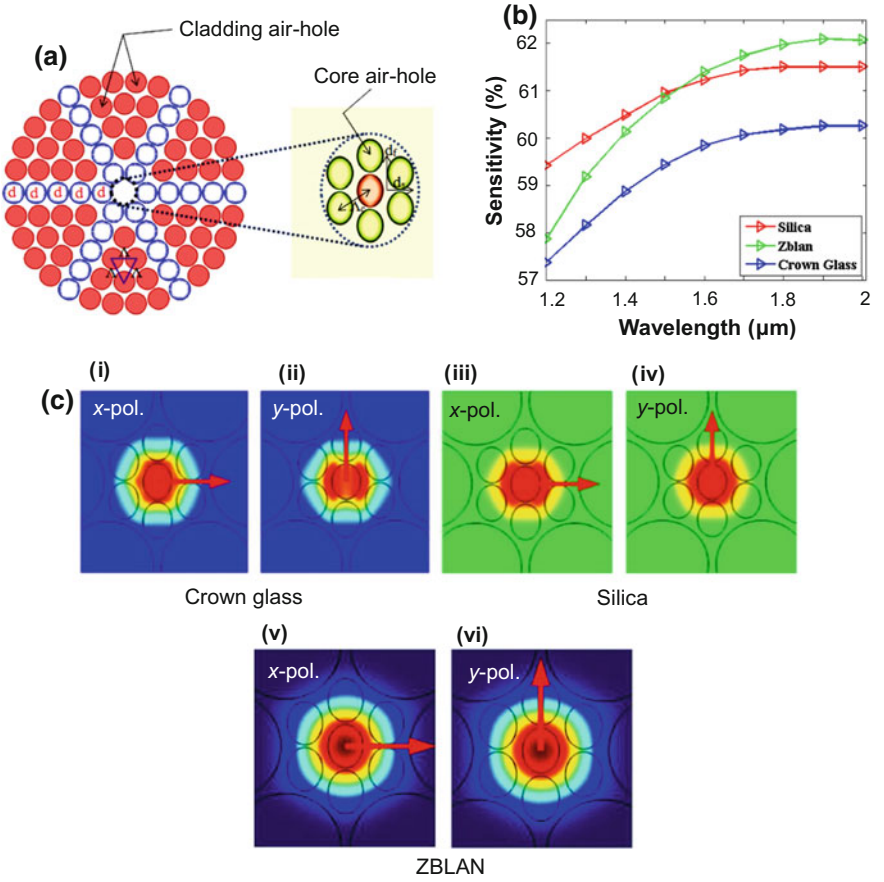

Fig. 12.24 **a** Cross-sectional view of the PCF sensor, **b** sensitivity as a function of wavelength, and **c** core-guided fundamental mode with different background materials i and ii crown glass, iii and iv silica, and v and vi ZBLAN [78]

becoming more popular. Moreover, toxic and harmful gases and chemicals are injurious and can cause an exploitation. Optical sensor more specifically photonic crystal fiber-based sensors has proved its ability to detect toxic gases and chemicals. Although numerous computational works have been done for PCF-based gas/chemical sensing, only a limited number of works have been explored experimentally. Additional experimental investigations are required to practically implement the PCF-based gas/chemical sensors.

The future aspects of the PCF-based gas/chemical sensors are as follows

- Need to simplify the PCF structure so that it can easily be fabricated.
- For PCF-based gas/chemical sensors, core region is very important because generally, gases and chemicals are flow through the core. A result needs to make a suitable core structure to absorb the light as much as possible.
- The propagation loss needs to control which is important for the practical realization. Otherwise, light will immediately vanish after launching the light one end of the fiber; as a result, it will not able to generate the measurable signal at the output end.
- Selective gas/chemical infiltrations are required in most of the reported PCF-based gas/chemical sensors. This is another challenge issue for practical realization. Its alternative solution could be external gas/chemical-sensing approaches.

References

1. T.N. Do, Y. Visell, Stretchable, twisted conductive microtubules for wearable computing, robotics, electronics, and healthcare. Sci. Rep. **7** (2017)
2. D. Ahuja, D. Parande, Optical sensors and their applications. J. Sci. Res. Rev. **1**, 060–068 (2012)
3. J.C. Yeo, C.T. Lim, Emerging flexible and wearable physical sensing platforms for healthcare and biomedical applications. Microsyst. Nanoeng. **2** (2016)
4. S.A. Morin, R.F. Shepherd, S.W. Kwok, A.A. Stokes, A. Nemiroski, G.M. Whitesides, Camouflage and display for soft machines. Science **337**, 828–832 (2012)
5. S. Gong, W. Schwalb, Y. Wang, Y. Chen, Y. Tang, J. Si et al., A wearable and highly sensitive pressure sensor with ultrathin gold nanowires. Nat. Commun. **5**, 3132 (2014)
6. S. Xu, Y. Zhang, L. Jia, K.E. Mathewson, K.-I. Jang, J. Kim et al., Soft microfluidic assemblies of sensors, circuits, and radios for the skin. Science **344**, 70–74 (2014)
7. M. Kaltenbrunner, T. Sekitani, J. Reeder, T. Yokota, K. Kuribara, T. Tokuhara et al., An ultra-lightweight design for imperceptible plastic electronics. Nature **499**, 458 (2013)
8. I.E. Araci, B. Su, S.R. Quake, Y. Mandel, An implantable microfluidic device for self-monitoring of intraocular pressure. Nat. Med. **20**, 1074–1078 (2014)
9. W. Ding, Y. Jiang, R. Gao, Y. Liu, High-temperature fiber-optic Fabry-Perot interferometric sensors. Rev. Sci. Instrum. **86**, 055001 (2015)
10. S. Liu, K. Yang, Y. Wang, J. Qu, C. Liao, J. He et al., High-sensitivity strain sensor based on in-fiber rectangular air bubble. Sci. Rep. **5**, 7624 (2015)
11. Y. Liu, D. Wang, W. Chen, Crescent shaped Fabry-Perot fiber cavity for ultra-sensitive strain measurement. Sci. Rep. **6** (2016)
12. S. Asaduzzaman, B.K. Paul, K. Ahmed, Enhancement of sensitivity and birefringence of a gas sensor on micro-core based photonic crystal fiber, in *2016 3rd International Conference on Electrical Engineering and Information Communication Technology (ICEEICT)* (2016), pp. 1–4
13. N.L. Andrews, R. Ross, D. Munzke, C. van Hoorn, A. Brzezinski, J.A. Barnes et al., In-fiber Mach-Zehnder interferometer for gas refractive index measurements based on a hollow-core photonic crystal fiber. Opt. Express **24**, 14086–14099 (2016)
14. X. Feng, W. Feng, C. Tao, D. Deng, X. Qin, R. Chen, Hydrogen sulfide gas sensor based on graphene-coated tapered photonic crystal fiber interferometer. Sens. Actuators B Chem. **247**, 540–545 (2017)

15. Y. Zhao, Z.-Q. Deng, J. Li, Photonic crystal fiber based surface plasmon resonance chemical sensors. Sens. Actuators B Chem. **202**, 557–567 (2014)
16. T.A. Birks, J.C. Knight, P.S.J. Russell, Endlessly single-mode photonic crystal fiber. Opt. Lett. **22**, 961–963 (1997)
17. R. Cregan, B. Mangan, J. Knight, T. Birks, P.S.J. Russell, P. Roberts et al., Single-mode photonic band gap guidance of light in air. Science **285**, 1537–1539 (1999)
18. M. Arjmand, R. Talebzadeh, Optical filter based on photonic crystal resonant cavity. Optoelectron. Adv. Mater.-Rapid Commun. **9**, 32–35 (2015)
19. K. Fasihi, High-contrast all-optical controllable switching and routing in nonlinear photonic crystals. J. Lightwave Technol. **32**, 3126–3131 (2014)
20. K. Cui, Q. Zhao, X. Feng, Y. Huang, Y. Li, D. Wang et al., Thermo-optic switch based on transmission-dip shifting in a double-slot photonic crystal waveguide. Appl. Phys. Lett. **100**, 201102 (2012)
21. J.-M. Brosi, C. Koos, L.C. Andreani, M. Waldow, J. Leuthold, W. Freude, High-speed low-voltage electro-optic modulator with a polymer-infiltrated silicon photonic crystal waveguide. Opt. Express **16**, 4177–4191 (2008)
22. Y. Gao, R.-J. Shiue, X. Gan, L. Li, C. Peng, I. Meric et al., High-speed electro-optic modulator integrated with graphene-boron nitride heterostructure and photonic crystal nanocavity. Nano Lett. **15**, 2001–2005 (2015)
23. H. Xuan, J. Ma, W. Jin, W. Jin, Polarization converters in highly birefringent microfibers. Opt. Express **22**, 3648–3660 (2014)
24. Y.-H. Chang, Y.-Y. Jhu, C.-J. Wu, Temperature dependence of defect mode in a defective photonic crystal. Opt. Commun. **285**, 1501–1504 (2012)
25. Y. Liu, H. Salemink, All-optical on-chip sensor for high refractive index sensing in photonic crystals. EPL (Europhys. Lett.) **107**, 34008 (2014)
26. A.A. Rifat, R. Ahmed, A.K. Yetisen, H. Butt, A. Sabouri, G.A. Mahdiraji et al., Photonic crystal fiber based plasmonic sensors. Sens. Actuators B Chem. **243**, 311–325 (2017)
27. P. Hu, X. Dong, W.C. Wong, L.H. Chen, K. Ni, C.C. Chan, Photonic crystal fiber interferometric pH sensor based on polyvinyl alcohol/polyacrylic acid hydrogel coating. Appl. Opt. **54**, 2647–2652 (2015)
28. A.A. Rifat, M.R. Hasan, R. Ahmed, H. Butt, Photonic crystal fiber-based plasmonic biosensor with external sensing approach. J. Nanophotonics **12**, 012503 (2017)
29. M. Pushkarsky, M. Webber, O. Baghdassarian, L. Narasimhan, C.K.N. Patel, Laser-based photoacoustic ammonia sensors for industrial applications. Appl. Phys. B Lasers Opt. **75**, 391–396 (2002)
30. G. Whitenett, G. Stewart, K. Atherton, B. Culshaw, W. Johnstone, Optical fibre instrumentation for environmental monitoring applications. J. Opt. A Pure Appl. Opt. **5**, S140 (2003)
31. J.P. Carvalho, H. Lehmann, H. Bartelt, F. Magalhães, R. Amezcua-Correa, J.L. Santos, et al., Remote system for detection of low-levels of methane based on photonic crystal fibres and wavelength modulation spectroscopy. J. Sens. **2009** (2009)
32. R.A. Aoni, R. Ahmed, M.M. Alam, and S. Razzak, Optimum design of a nearly zero ultra-flattened dispersion with lower confinement loss photonic crystal fibers for communication systems. Int. J. Sci. Eng. Res. **4** (2013)
33. M.S. Habib, M.S. Habib, S.A. Razzak, M.A. Hossain, Proposal for highly birefringent broadband dispersion compensating octagonal photonic crystal fiber. Opt. Fiber Technol. **19**, 461–467 (2013)
34. S.A. Razzak, M.A.G. Khan, F. Begum, S. Kaijage, Guiding properties of a decagonal photonic crystal fiber. J. Microwaves Optoelectron. Electromagn. Appl. (JMOe) **6**, 44–49 (2007)
35. R. Ahmmed, R. Ahmed, S.A. Razzak, Design of large negative dispersion and modal analysis for hexagonal, square, FCC and BCC photonic crystal fibers, in *2013 International Conference on Informatics, Electronics & Vision (ICIEV)* (2013), pp. 1–6.
36. Y. Hou, F. Fan, Z.-W. Jiang, X.-H. Wang, S.-J. Chang, Highly birefringent polymer terahertz fiber with honeycomb cladding. Opt. Int. J. Light Electron Opt. **124**, 3095–3098 (2013)

37. R. Hao, Z. Li, G. Sun, L. Niu, Y. Sun, Analysis on photonic crystal fibers with circular air holes in elliptical configuration. Opt. Fiber Technol. **19**, 363–368 (2013)
38. M.R. Hasan, S. Akter, T. Khatun, A.A. Rifat, M.S. Anower, Dual-hole unit-based kagome lattice microstructure fiber for low-loss and highly birefringent terahertz guidance. Opt. Eng. **56**, 043108–043108 (2017)
39. J. Hecht, *Understanding fiber optics* (Jeff Hecht, 2015)
40. E. Udd, Fiber optic sensors based on the Sagnac interferometer and passive ring resonator. Fiber opt. Sens. Introduc.Eng. Sci. (1991)
41. P. Sharan, S. Bharadwaj, F.D. Gudagunti, P. Deshmukh, Design and modelling of photonic sensor for cancer cell detection, in *2014 International Conference on the IMpact of E-Technology on US (IMPETUS)* (2014), pp. 20–24.
42. J. Park, S. Lee, S. Kim, K. Oh, Enhancement of chemical sensing capability in a photonic crystal fiber with a hollow high index ring defect at the center. Opt. Express **19**, 1921–1929 (2011)
43. S. Olyaee, A. Naraghi, V. Ahmadi, High sensitivity evanescent-field gas sensor based on modified photonic crystal fiber for gas condensate and air pollution monitoring. Opt. Int. J. Light Electron Opt. **125**, 596–600 (2014)
44. H. Ademgil, Highly sensitive octagonal photonic crystal fiber based sensor. Opt. Int. J. Light Electron Opt. **125**, 6274–6278 (2014)
45. W. Jin, H. Ho, Y. Cao, J. Ju, L. Qi, Gas detection with micro-and nano-engineered optical fibers. Opt. Fiber Technol. **19**, 741–759 (2013)
46. E. Austin, A. van Brakel, M.N. Petrovich, D.J. Richardson, Fibre optical sensor for C 2 H 2 gas using gas-filled photonic bandgap fibre reference cell. Sens. Actuators B Chem. **139**, 30–34 (2009)
47. S. Asaduzzaman, K. Ahmed, Proposal of a gas sensor with high sensitivity, birefringence and nonlinearity for air pollution monitoring. Sens. Bio-Sens. Res. **10**, 20–26 (2016)
48. K. Ahmed, M. Morshed, Design and numerical analysis of microstructured-core octagonal photonic crystal fiber for sensing applications. Sens. Bio-Sens. Res. **7**, 1–6 (2016)
49. S. Asaduzzaman, K. Ahmed, T. Bhuiyan, T. Farah, Hybrid photonic crystal fiber in chemical sensing. SpringerPlus **5**, 748 (2016)
50. Q. Liu, S. Li, H. Chen, Z. Fan, J. Li, Photonic crystal fiber temperature sensor based on coupling between liquid-core mode and defect mode. IEEE Photonics J. **7**, 1–9 (2015)
51. Y. Lu, M. Wang, C. Hao, Z. Zhao, J. Yao, Temperature sensing using photonic crystal fiber filled with silver nanowires and liquid. IEEE Photonics J. **6**, 1–7 (2014)
52. Y. Al-Qazwini, A. Noor, Z. Al-Qazwini, M.H. Yaacob, S. Harun, M. Mahdi, Refractive index sensor based on SPR in symmetrically etched plastic optical fibers. Sens. Actuators A **246**, 163–169 (2016)
53. T. Takeo, H. Hattori, Optical fiber sensor for measuring refractive index. Jpn. J. Appl. Phys. **21**, 1509 (1982)
54. K. Cooper, J. Elster, M. Jones, R. Kelly, Optical fiber-based corrosion sensor systems for health monitoring of aging aircraft, in *2001 IEEE Systems Readiness Technology Conference on AUTOTESTCON Proceedings* (2001), pp. 847–856.
55. K.T. Wan, C.K. Leung, Durability tests of a fiber optic corrosion sensor. Sensors **12**, 3656–3668 (2012)
56. L. Alwis, T. Sun, K. Grattan, Optical fibre-based sensor technology for humidity and moisture measurement: review of recent progress. Measurement **46**, 4052–4074 (2013)
57. C. Bariain, I.R. Matías, F.J. Arregui, M. López-Amo, Optical fiber humidity sensor based on a tapered fiber coated with agarose gel. Sens. Actuators B Chem. **69**, 127–131 (2000)
58. D. Bykov, O. Schmidt, T. Euser, P.S.J. Russell, Flying particle sensors in hollow-core photonic crystal fibre. Nat. Photonics **9**, 461 (2015)
59. Y. Wang, N. Li, X. Huang, M. Wang, Fiber optic transverse load sensor based on polarization properties of π-phase-shifted fiber Bragg grating. Opt. Commun. **342**, 152–156 (2015)

60. M.S. Islam, B.K. Paul, K. Ahmed, S. Asaduzzaman, M.I. Islam, S. Chowdhury et al., Liquid-infiltrated photonic crystal fiber for sensing purpose: design and analysis. Alexandria Eng. J. (2017)
61. K. Ahmed, M.S. Islam, B.K. Paul, Design and numerical analysis: effect of core and cladding area on hybrid hexagonal microstructure optical fiber in environment pollution sensing applications. Karbala Int. J. Mod. Sci. **3**, 29–38 (2017)
62. W.L. Ng, A.A. Rifat, W.R. Wong, D.C. Tee, F.R. Mahamd Adikan, Enhancement of evanescent field exposure in a photonic crystal fibre with interstitial holes. J. Mod. Opt. **64**, 1544–1549 (2017)
63. A.A. Rifat, R. Ahmed, G.A. Mahdiraji, F.M. Adikan, highly sensitive d-shaped photonic crystal fiber-based plasmonic biosensor in visible to near-IR. IEEE Sens. J. **17**, 2776–2783 (2017)
64. M. De, R.K. Gangwar, V.K. Singh, Designing of highly birefringence, dispersion shifted decagonal photonic crystal fiber with low confinement loss. Photonics Nanostruct. Fundam. Appl. **26**, 15–23 (2017)
65. L. Xin, L. Ying, X. Guo, Modular interference characteristics and beat length of a two-hole photonic crystal fiber, in *International Symposium on Optoelectronic Technology and Application 2016* (2016), pp. 101550T–101550T-7
66. M.R. Hasan, M.A. Islam, A.A. Rifat, A single mode porous-core square lattice photonic crystal fiber for THz wave propagation. J. Eur. Opt. Soc. Rapid Publ. **12**, 15 (2016)
67. S.K. Mishra, S. Rani, B.D. Gupta, Surface plasmon resonance based fiber optic hydrogen sulphide gas sensor utilizing nickel oxide doped ITO thin film. Sens. Actuators B Chem. **195**, 215–222 (2014)
68. S.K. Mishra, S. Bhardwaj, B.D. Gupta, Surface plasmon resonance-based fiber optic sensor for the detection of low concentrations of ammonia gas. IEEE Sens. J. **15**, 1235–1239 (2015)
69. S. Asaduzzaman, K. Ahmed, M.F.H. Arif, M. Morshed, Proposal of a simple structure photonic crystal fiber for lower indexed chemical sensing, in *2015 18th International Conference on Computer and Information Technology (ICCIT)* (2015), pp. 127–131
70. M. Morshed, S. Asaduzzaman, M.F.H. Arif, K. Ahmed, Proposal of simple gas sensor based on micro structure optical fiber in *2015 International Conference on Electrical Engineering and Information Communication Technology (ICEEICT)* (2015), pp. 1–5
71. S. Das, V. Jayaraman, SnO 2: a comprehensive review on structures and gas sensors. Prog. Mater Sci. **66**, 112–255 (2014)
72. S. Asaduzzaman, K. Ahmed, B.K. Paul, Slotted-core photonic crystal fiber in gas-sensing application, in *SPIE/COS Photonics Asia* (2016), pp. 100250O–100250O-9
73. S. Asaduzzaman, M.F.H. Arif, K. Ahmed, P. Dhar, Highly sensitive simple structure circular photonic crystal fiber based chemical sensor, in *2015 IEEE International WIE Conference on Electrical and Computer Engineering (WIECON-ECE)* (2015), pp. 151–154
74. S. Asaduzzaman, K. Ahmed, M.F.H. Arif, M. Morshed, Application of microarray-core based modified photonic crystal fiber in chemical sensing, in *2015 International Conference on Electrical & Electronic Engineering (ICEEE)* (2015), pp. 41–44
75. J.-P. Berenger, A perfectly matched layer for the absorption of electromagnetic waves. J. Comput. Phys. **114**, 185–200 (1994)
76. T. Uno, Y. He, S. Adachi, Perfectly matched layer absorbing boundary condition for dispersive medium. IEEE Microwave Guided Wave Lett. **7**, 264–266 (1997)
77. B.K. Paul, K. Ahmed, S. Asaduzzaman, M.S. Islam, Folded cladding porous shaped photonic crystal fiber with high sensitivity in optical sensing applications: design and analysis. Sens. Bio-Sens. Res. **12**, 36–42 (2017)
78. K. Ahmed, I. Islam, B.K. Paul, S. Islam, S. Sen, S. Chowdhury et al., Effect of photonic crystal fiber background materials in sensing and communication applications. Mat. Discov. (2017)
79. G. Amouzad Mahdiraji, D.M. Chow, S. Sandoghchi, F. Amirkhan, E. Dermosesian, K.S. Yeo et al., Challenges and solutions in fabrication of silica-based photonic crystal fibers: an experimental study. Fiber Integr. Opt. **33**, 85–104 (2014)

80. R.T. Bise, D. Trevor, Solgel-derived microstructured fibers: fabrication and characterization, in *Optical Fiber Communication Conference* (2005), p. OWL6
81. H. El Hamzaoui, Y. Ouerdane, L. Bigot, G. Bouwmans, B. Capoen, A. Boukenter et al., Sol-gel derived ionic copper-doped microstructured optical fiber: a potential selective ultraviolet radiation dosimeter. Opt. Express **20**, 29751–29760 (2012)
82. H. Ebendorff-Heidepriem, P. Petropoulos, S. Asimakis, V. Finazzi, R.C. Moore, K. Frampton et al., Bismuth glass holey fibers with high nonlinearity. Opt. Express **12**, 5082–5087 (2004)
83. J. Knight, T. Birks, P.S.J. Russell, D. Atkin, All-silica single-mode optical fiber with photonic crystal cladding. Opt. Lett. **21**, 1547–1549 (1996)